Supporting Information For: Direct Optical Determination of Interfacial Transport Barriers in Molecular Tunnel Junctions

Jerry A. Fereiro[1], Richard L. McCreery[*1,2], and Adam Johan Bergren[*2]

[1]Department of Chemistry, University of Alberta, Edmonton, AB

[2]National Institute for Nanotechnology, National Research Council Canada

*Correspondence to: richard.mccreery@ualberta.ca (RLM); adam.bergren@nrc.ca (AJB)

Introduction

This document contains additional supporting data, figures, discussions, and equations used to support the main text. Specifically:

1. Plot of Yield vs. Wavelength
2. Junction Fabrication, Molecular Thickness, and Electronic Characteristics
3. Experimental Photocurrent Measurement Setup
4. Calibration: Conversion of Photocurrent to Yield and Phase Calibration
5. Analysis of Bolometric Mechanism
6. Analysis of Background Current and Direct PPF/Cu Contact
7. UPS for C12 and BrP
8. UV-vis absorption spectra of chemisorbed molecules

1. Plot of Yield versus wavelength (modified form of Figure 2 in the main text).

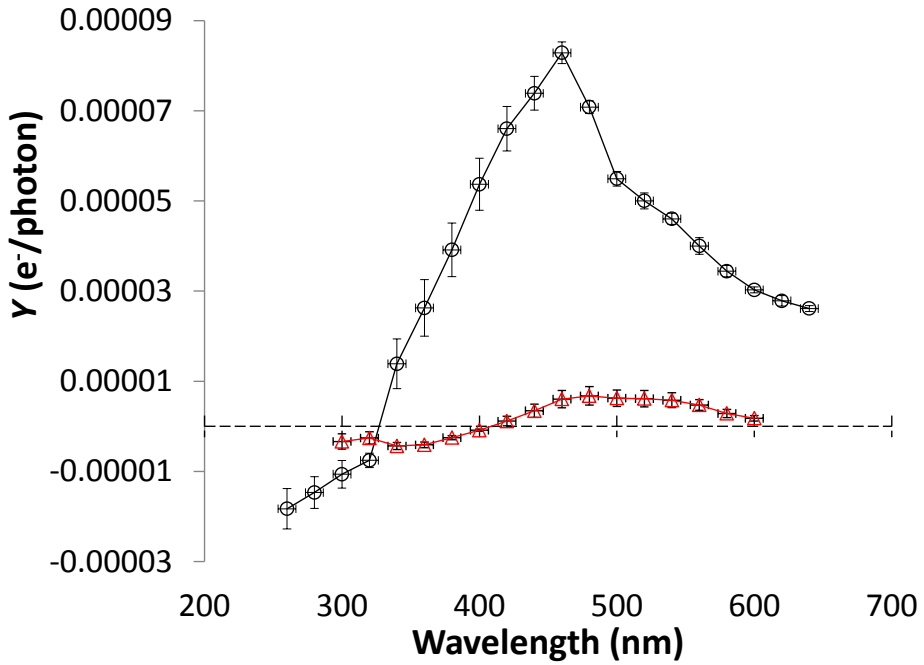

Figure S1. Data from Figure 2 plotted with wavelength on the abscissa for molecular junctions containing alkane (red triangles) and bromophenyl (black circles) molecular layers.

2. Junction Fabrication, Molecular Thickness, and Electronic Characteristics

In order to ensure against any background current arising from stray photo conductance, polished fused quartz wafers (Technical Glass Products, http://www.technicalglass.com/) were diced into 1.2 x 1.5 cm chips to serve as substrates. Conductive carbon in the form of pyrolyzed photoresist films (PPF) were produced by first spin-coating commercially available photoresist (AZ-P4330-RS) onto pre-cleaned (by sonication in acetone, isopropanol, and water for 10 min each) quartz chips[1,2]. Next, the photoresist was patterned using photolithography to yield four parallel 0.5 mm wide lines. Finally, the photoresist was converted to conductive carbon by heating to 1100° C in a tube furnace with a constant 100 sccm flow of forming gas (5% H_2, balance N_2). PPF is a flat (RMS roughness <0.5 nm measured by AFM) and electrically conductive (resistivity ~0.005 Ω cm) substrate upon which molecules are bonded[1].

Formation of molecular layers ranging from 1-5 nm thickness was carried out by electrochemical reduction of diazonium ions in solution. Here, PPF was used as the working electrode in a three-electrode electrochemical cell with a 1 mM solution of the diazonium precursor with 0.1 M tetrabutylammonium tetrafluroborate ($TBABF_4$) as the supporting electrolyte in acetonitrile. To deposit the molecular layer, cyclic voltammetric sweeps starting from +0.4 V versus Ag/Ag^+ to -1.1 V were repeated ten times. After modification, the sample was rinsed with acetonitrile and dried using a stream of nitrogen.

The derivatization of PPF with aminododecane (C12) was performed by amine oxidation. First, a solution of 5 mM aminododecane in acetonitrile with 0.1 M $TBABF_4$ was stirred for 1 hour. Next, using the PPF as a working electrode, +1.4 V vs. Ag/Ag^+ was applied for 12 min[3] to obtain thicknesses of 2.3 nm. Initial and final scans were swept from 0 to +1.4 respectively, before and after CPE to check for the passivation of the PPF surface[3,4].

Finally, top contact deposition was carried out via electron beam evaporation through a shadow mask with 0.25 mm openings oriented perpendicular to the PPF lines, which results in a cross bar junction of ~0.00125cm^2 area.

For UV absorption measurements in a Perkin Elmer 900 spectrometer, optically transparent PPF on quartz was utilized[5,6]. Fabrication follows the same procedure outlined above, but employs photoresist diluted to a concentration of 5% (v/v) with propylene glycol methyl ether acetate as the solvent, without a photolithography step. These electrodes maintained sufficient conductivity for electrochemistry, enabling modification of the surface via diazonium ion reduction [6], with derivatization carried out as outlined above.

Measurement of molecular layer thickness was done using AFM, using the same procedure described in the supplementary data from reference [7]. Table S1 lists the thicknesses determined for the samples reported in this work, along with their standard deviation.

Table S1. Summary of the different type of molecules used, and their measured thickness and standard deviation data from the AFM measurements.

Molecule	Thickness (nm)	Standard Deviation(nm)
$CH_3(CH_2)_{11}NH$- (C12)	2.26	0.79
Bromophenyl (BrP)	2.99	0.37

Finally, the electronic characteristics of the molecular junctions were measured, with results shown in Figure S2. These results indicate that the molecular junctions are not short circuits, which result in linear *J-V* curves, but instead result from tunneling across the molecular layer. We note that when linear *J-V* curves are observed, the photocurrent signal is absent or very weak, as shown in Section 6 below.

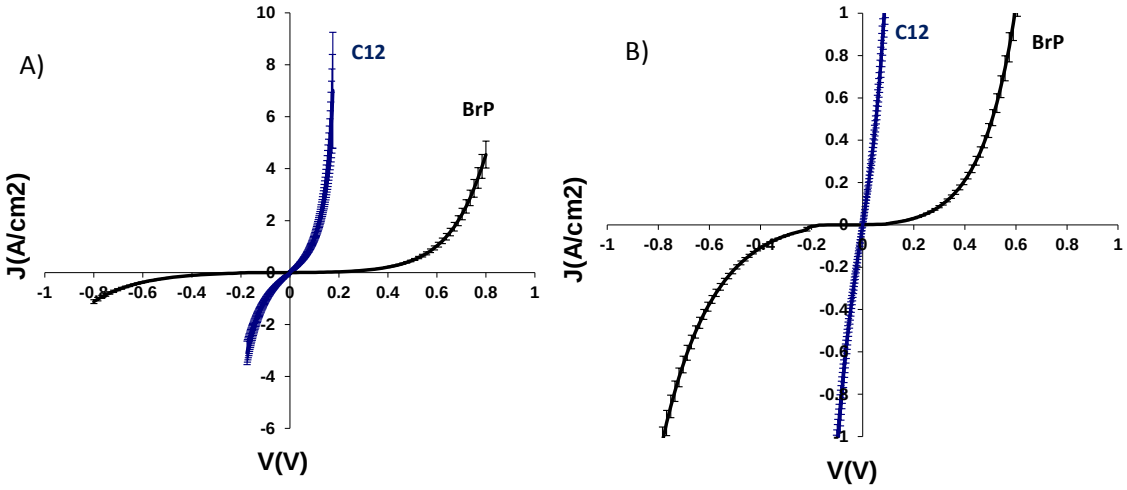

Figure S2. (A) *J-V* curves for a series of BrP and C12 junction showing the C12 response on full scale. (B) Expanded ordinate showing the BrP response. Error bars represent one standard deviation for four junctions.

3. Experimental Photocurrent Measurement Setup

Figure S3 shows a diagram of the measurement set up using a 150 W Xenon arc lamp (Newport model 6256) as the source of illumination. After passing through a model 74004 Cornerstone 130 1/8 m motorized monochromator (bandpass = 13 nm), the selected wavelength was chopped at frequency ω. The chopped light was then directed through a series of lenses and mirrors for focussing, as shown in Figure S3. The PPF contact was connected via a tungsten probe and shielded cable to the AC-coupled current input of a dual phase lock-in amplifier (LIA, Stanford-830), and the shield was connected to the Cu contact of the molecular junction. The output from the LIA was recorded using a Labview data acquisition program. In all cases, the PPF was considered the positive terminal, as shown in Figure 1 of the main text.

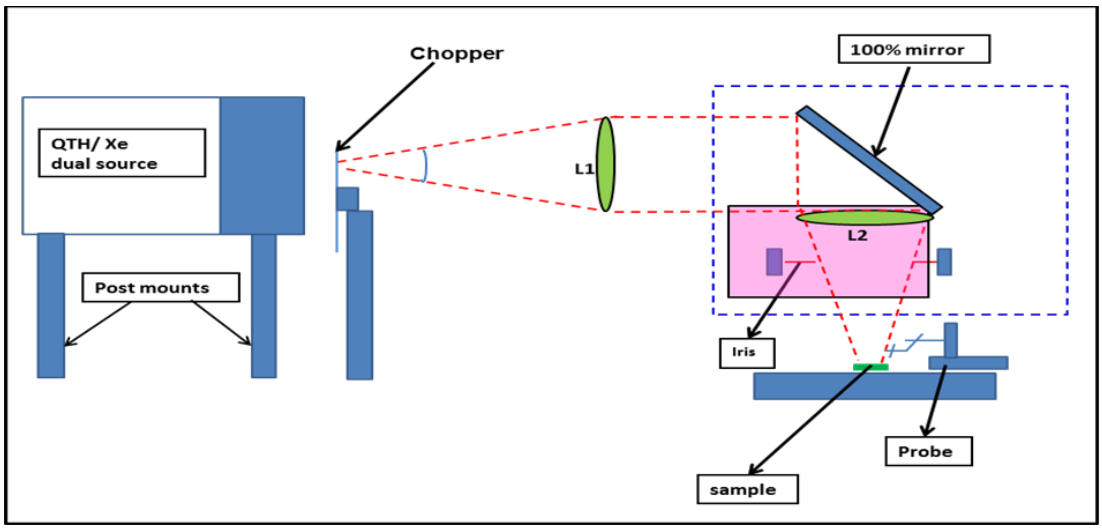

Figure S3. The experimental set up used for the arc source.

4. Calibration: Conversion of Photocurrent to Yield and Phase Calibration

In order to determine the quantum yield for photocurrent generation, the power incident onto the junction was determined at each wavelength using a Newport power meter (Model 1936-R). The power density as a function of wavelength is given in Figure S4, and was periodically verified. The beam power density (P_b, in W cm^{-2}) was then calculated by dividing

the observed power by the beam area (0.0576 cm^2). Since the beam area is much larger than the junction area (A_j = 0.0012 cm^2), the total power incident onto the junction was P_b x A_j, with visual inspection (a magnified camera view) and micrometer-controlled stage used to ensure proper junction positioning.

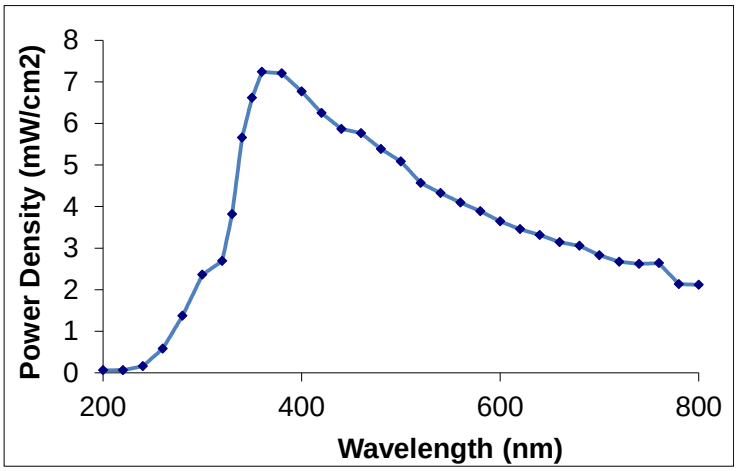

Figure S4. Power density of Xe arc/monochromator with bandpass of 13 nm, measured at the sample position.

Photon flux (*pf*, photons per second incident onto the junction) is given by

$$pf = \frac{P_b A_j}{h\nu} \quad \text{(S1)}$$

where *h* is Plank's constant (6.62607 x 10^{-34} J s) and ν is the frequency of the incident light (c/λ). The measured photocurrent was converted to electron flux, *ef* (e^- per second):

$$ef = \frac{i_p}{q} \quad \text{(S2)}$$

where *q* is the elementary charge (1.60218 x 10^{-19} C/e). Finally, yield (*Y*, in e^- per photon incident on the junction) is calculated by

$$Y = \frac{ef}{pf} \quad \text{(S3)}$$

Since photocurrent measured using the setup in Figure S3 gives only the magnitude of the current, the sign was determined through a phase calibration. For this purpose, we employed a photodiode (Advanced Photonix P/N: PDB-C613-2, response time 50 ns), wired so that a

positive photocurrent resulted from illumination (see Figure S5A). Since the response time of the photodiode is much faster than the chopping frequency, the LIA reference phase was adjusted to read zero degrees for the illuminated photodiode. By keeping the geometry and other variables constant and replacing the photodiode with a molecular junction, the sign of the photocurrent can be determined from the phase output of the LIA. For example, when the phase remains near zero, the photocurrent is positive, with the molecular junctions exhibiting the same polarity as the photodiode. Conversely, a phase output of 180^{o} indicates negative photocurrent. We have defined a negative photocurrent for cases where the phase is between -90° and -180°, while positive photocurrent is taken for 0° to -90°. Figure S6 shows the phase as measured for two junctions, where the black curve represents BrP, and the red curve is data for C12. As defined above, negative photocurrent occurs for BrP above 3.8 eV, while for C12 the transition takes place at 3 eV. These results were verified for molecular junctions using laser illumination at 780 nm (1.59 eV). The increased intensity available with the laser excitation enabled direct DC measurement of the photocurrent (no LIA). Figure S5B shows the result for a BrP junction, showing a positive photocurrent for 1.59 eV photons, consistent with Figure S6 at this energy. Similar comparisons of DC and LIA responses were also consistent for a variety of molecules and laser wavelengths after phase calibration with a photodiode.

Figure S7A shows a plot of the phase angle recorded for the C12 junction as a function of chopper frequency for three different energies, showing that the phase response is not time-dependent within the chopper frequency range. For comparison, Figure S7B shows the response of a photodiode as a function of chopper frequency at 3.1 eV (similar curves were obtained for all energies).

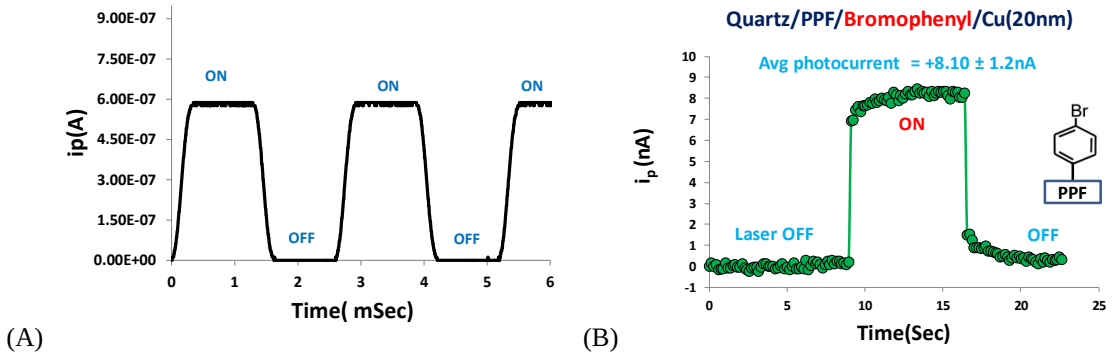

Figure S5. (A) Response of photodiode used for phase calibration on an oscilloscope. (B) Direct DC measurement of photocurrent for a BrP junction using 780 nm (1.59 eV) laser illumination in order to verify the phase calibration. For this case, the photocurrent sign is positive.

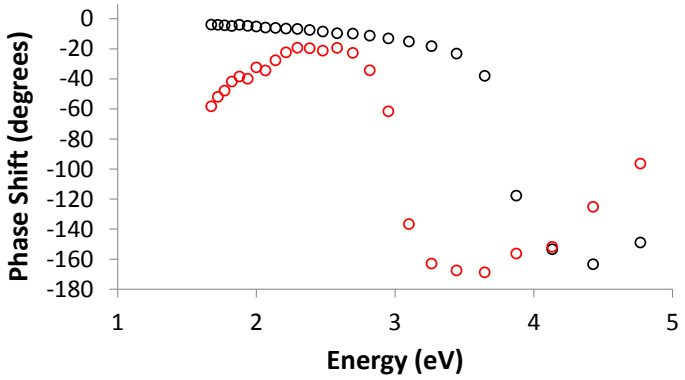

Figure S6. Measured phase angle as a function of energy for two different molecules shown in the main text (black curve is BrP, red curve is C12).

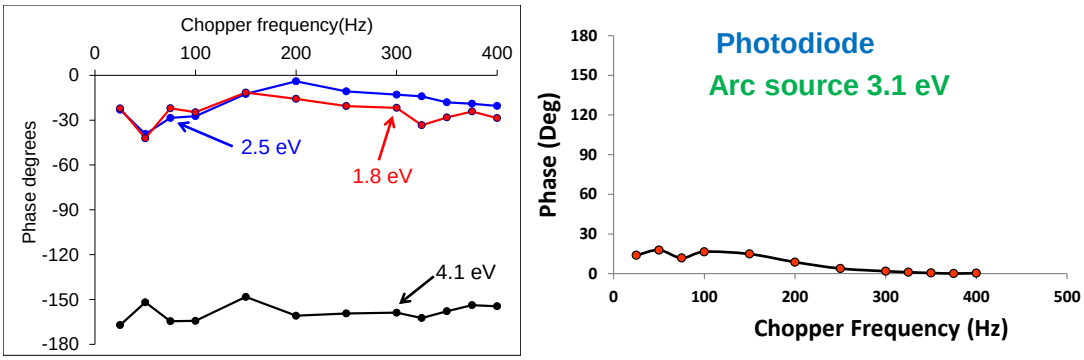

Figure S7. (A) Phase angle as a function of chopper frequency for C12 junction at three different photon energies, illustrating that a given phase angle is not dependent. (B) Same plot for a photodiode at 3.1 eV.

5. Analysis of Bolometric Mechanism

Because incident light absorption produces heat, we have carried out various tests to assess the possibility of heat-induced currents in molecular junctions. Initially, we observed excellent stability and a response time faster than the mechanical limit imposed by the chopper. As shown in Figure S8, a response time faster than 250 μs was observed.

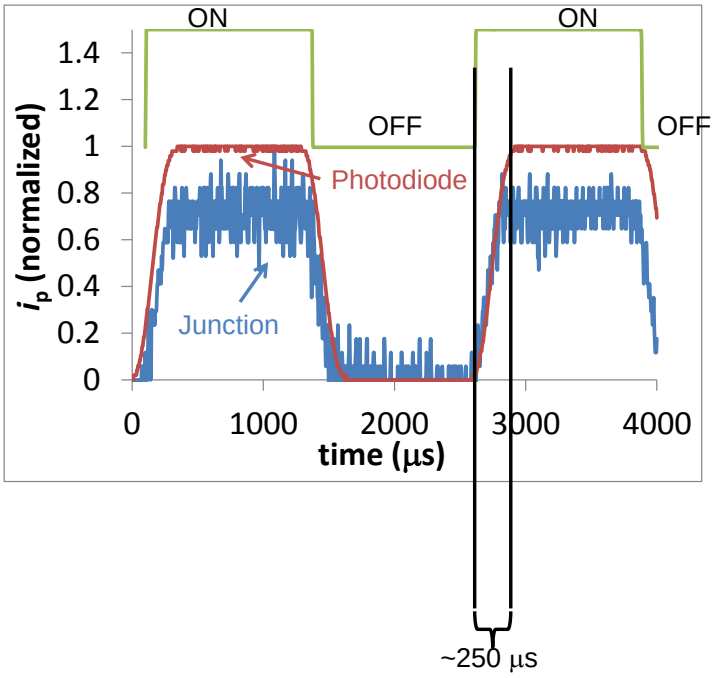

Figure S8. Oscilloscope trace of photocurrent versus time for 400 nm wavelength at 400 Hz for a photodiode (red curve) and a molecular junction (blue curve), showing that the response time of the molecular junction is faster than 250 μs. This time limit is due to the mechanical limit of the chopper wheel in the experimental setup, shown by the overlay of the photodiode response, which has a response time of 50 ns, but shows a similar rise time to the molecular junction.

An additional test for heat-induced currents is the dependence of the photocurrent on the chopping frequency. According to literature[8], heat-related photocurrent is expected to decrease with increasing chopping frequency, by the factor $f_{chop}^{-1.5}$. As shown in Figure S7, the phase angle is not frequency dependent, and Figure S9 shows that the photocurrent itself clearly does not follow an $f_{chop}^{-1.5}$ dependence for the molecular junctions studied here. In addition, the overlay of the response for the photodiode (response time 50 ns) indicates that the small changes

observed in the photocurrent as a function of chopping frequency are likely due to mechanical and geometrical factors in the experimental setup. Collectively, the results in Figure S7-S9 and the linearity of the Fowler plots in the main text indicate that heat is not likely to be responsible for the photocurrents reported here.

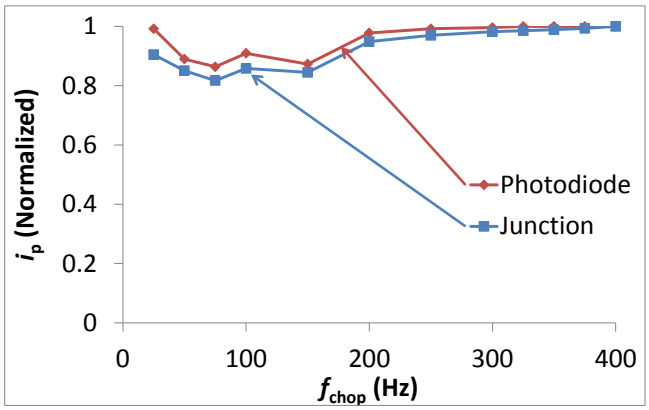

Figure S9. Variation of the measured photocurrent for a molecular junction (red curve) and photodiode (blue curve).

6. Analysis of Background Current and Direct PPF/Cu Contact

In order to determine the effect of the molecular structure further, tests were carried out with PPF/Cu junctions where no molecular layer was deposited. These junctions resulted in short circuits that display very high conductivity and linear *i-V* characteristics (in contrast to those shown in Figure S1). Prior to measuring the photocurrent for PPF/Cu, contact was verified to ensure a genuine response was obtained. The photocurrent was recorded using the same settings for all equipment as that used to record the responses shown in the main text. In addition, the response was obtained with and without illumination to determine the effect of background noise and determine if any other response results for PPF/Cu short circuits.

Figures S10A-C shows the results of these experiments. The PPF/Cu junction shows an indistinguishable response with and without illumination (Figure S10C) that is distinct from the

response obtained using a non-shorted molecular junction (Figures S10A-B). Figure S10D is a reproduction of Figure 2 of the main text, illustrating the energy ranges where a molecular junction response above the background current level is obtained. The Fowler analysis was conducted within this range, as shown in Figure 3 of the main text.

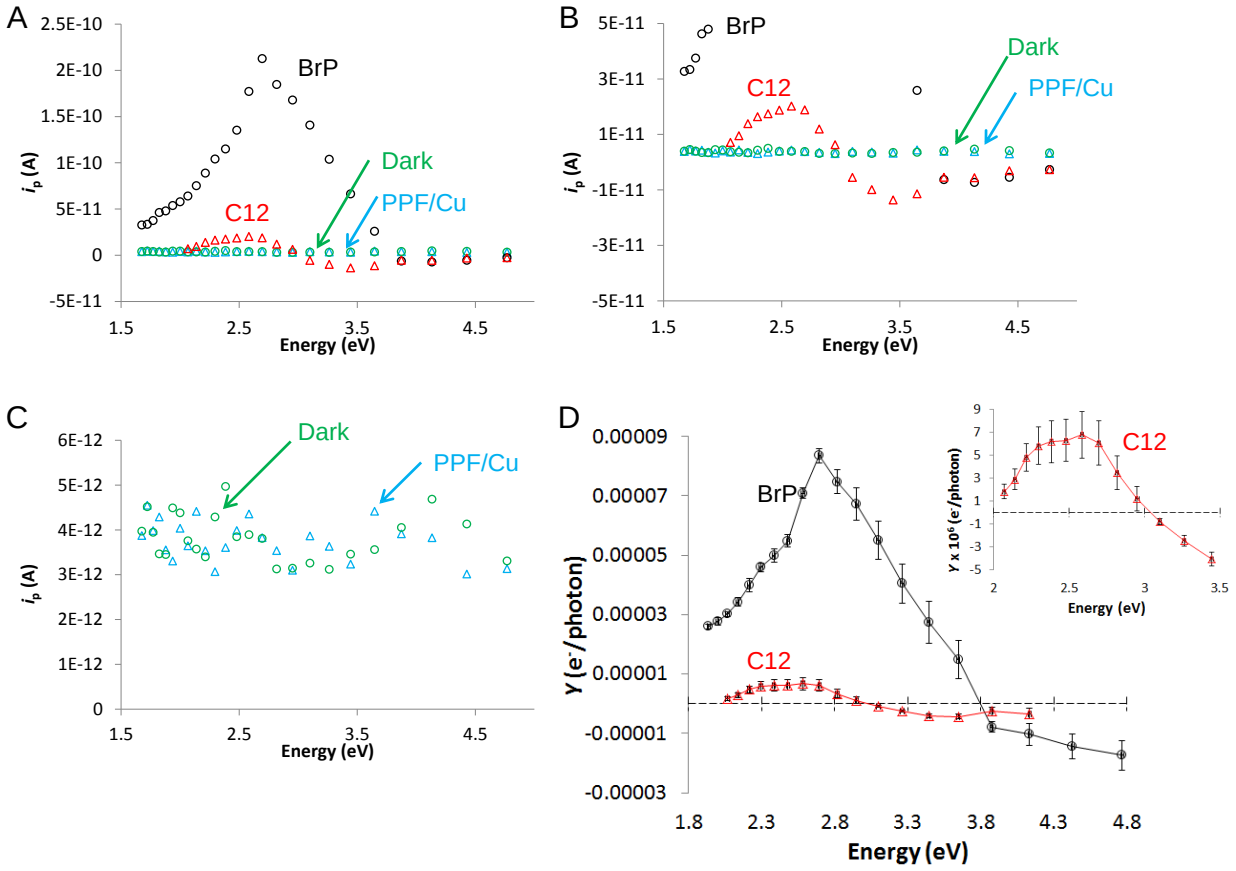

Figure S10. (A) Raw photocurrent versus energy for the entire range collected (260-740 nm or 1.68-4.77 eV) for four different cases: BrP (black circles) and C12 (red triangles) junctions and a PPF/Cu contact (blue triangles) and the same junction without light illumination (shutter closed, green circles). (B) Expanded ordinate showing the energy ranges where the signal obtained from the molecular junctions is above background (in particular, this is only the case for C12 above 2.0 eV. (C) Expanded view of the PPF/Cu junction with (blue triangles) and without (green circles) illumination, showing that the signal is not derived only from contact heating. (D) Figure 2 of the main text, showing the Yield vs. Energy plot is obtained for regions where the signal is above the background current.

5. UPS for C12 and BrP

Ultraviolet Photoelectron Spectroscopy (UPS) was carried out to determine HOMO onset energies ($E_{HOMO,onset}$) for BrP and C12, as described previously[7,9]. The onset of photoemission for a modified surface above that for an unmodified substrate in the low binding energy portion of the spectra indicates the presence of occupied states, and this onset has been correlated with the hole tunneling barrier. Figure S11A shows that the $E_{HOMO,onset}$ value for C12 is 1.7 ± 0.2 eV, while that for BrP (Figure S11B) is 1.2 ± 0.3 eV. Both are in excellent agreement with IPE.

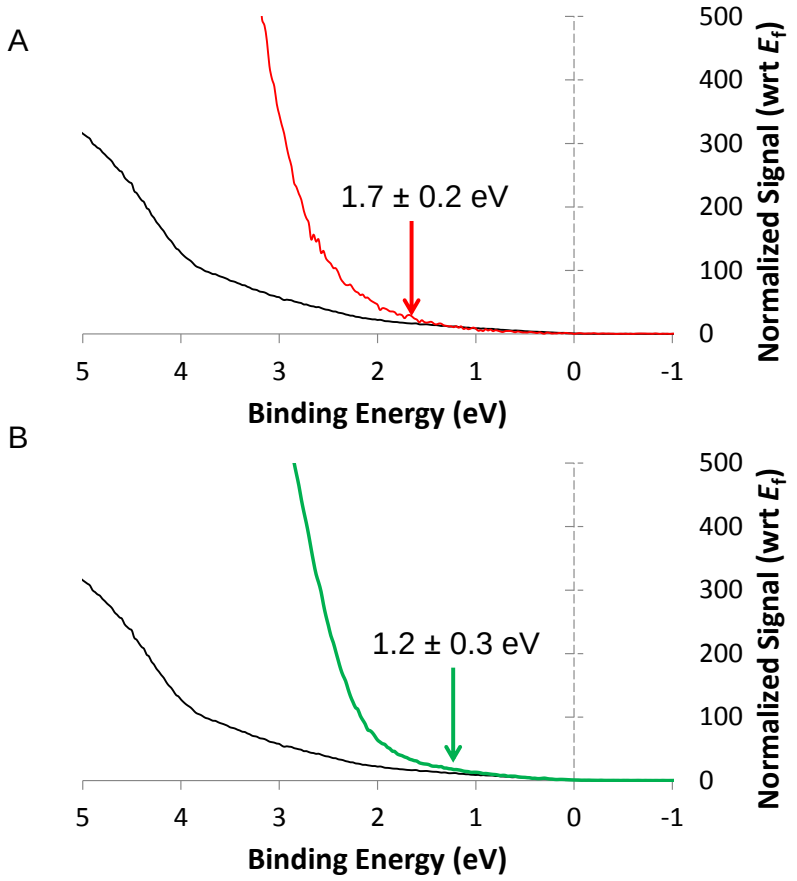

Figure S11. (A) UPS measurement of the HOMO onset energy for C12 on PPF. The value obtained (1.7 ± 0.2 eV) matches closely with the hole barrier obtained from IPE in the main text. (B) HOMO onset energy measurement for BrP, giving 1.2 ± 0.3 eV.

6. UV-vis Absorption Results

In order to ensure the IPE analysis is not obscured by the effects of molecular absorption, the optical absorbance spectra of the molecules bonded to PPF were obtained. Figure S12 shows the optical spectra for the two molecules discussed in the main text: C12 (blue curve) and BrP (black curve). The absorbance in Figure S12 was obtained by subtracting the absorbance of an unmodified quartz/carbon substrate (described above) from that of a similar substrate modified with the molecular layer[6]. It is clear that the C12 sample shows no significant optical absorbance over the entire range tested. The shift in the baseline absorbance is due to reflectance changes between the reference (unmodified transparent carbon) and the sample with the thin molecular layer, which has a refractive index different from air.

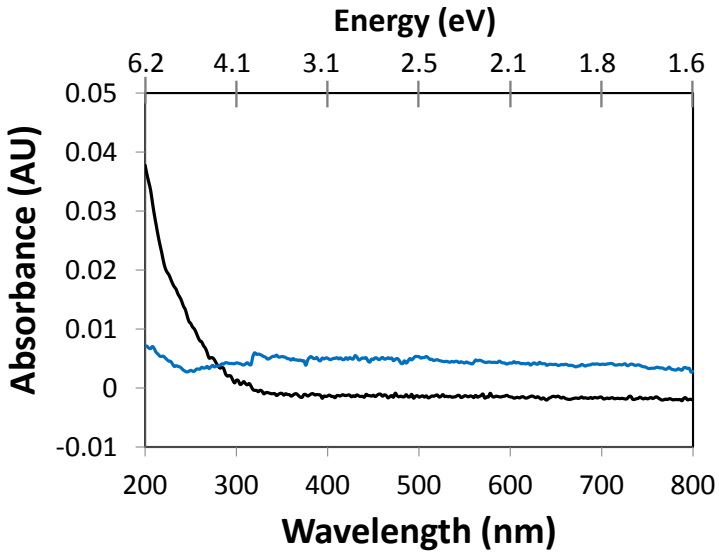

Figure S12. Overlay of the optical absorption spectra for the alkane (C12, blue curve) and bromophenyl (BrP, black curve) on optically transparent carbon.

References

(1) Ranganathan, S.; McCreery, R. L.; Majji, S. M.; Madou, M. *J. Electrochem. Soc.* **2000**, *147*, 277
(2) Ranganathan, S.; McCreery, R. L. *Anal. Chem.* **2001**, *73*, 893.
(3) Yan, H.; McCreery, R. L. *ACS Applied Materials & Interfaces* **2009**, *1*, 443.
(4) Deinhammer, R. S.; Ho, M.; Anderegg, J. W.; Porter, M. D. *Langmuir* **1994**, *10*, 1306.
(5) Donner, S.; Li, H. W.; Yeung, E. S.; Porter, M. D. *Anal. Chem.* **2006**, *78*, 2816.
(6) Tian, H.; Bergren, A. J.; McCreery, R. L. *Appl. Spectrosc.* **2007**, *61*, 1246.
(7) Sayed, S. Y.; Fereiro, J. A.; Yan, H.; McCreery, R. L.; Bergren, A. J. *Proc. Natl. Acad. Sci. U.S.A.* **2012**, *109*, 11498.
(8) Lee, C. H.; Yu, G.; Heeger, A. J. *Physical Review B* **1993**, *47*, 15543.
(9) Kim, B.; Choi, S. H.; Zhu, X. Y.; Frisbie, C. D. *J. Am. Chem. Soc.* **2011**, *133*, 19864.